On the origin of the differences in the Cu K-edge XANES of isostructural and isoelectronic compounds

2009 J. Phys.: Condens. Matter 21 255401

(http://iopscience.iop.org/0953-8984/21/25/255401)

J. Phys.: Condens. Matter **21** (2009) 255401 (9pp) doi:10.1088/0953-8984/21/25/255401

On the origin of the differences in the Cu K-edge XANES of isostructural and isoelectronic compounds

O Šipr[1], F Rocca[2] and P Fornasini[3]

[1] Institute of Physics, Academy of Sciences of the Czech Republic, Cukrovarnická 10, CZ-162 53 Prague, Czech Republic
[2] IFN-CNR, Istituto di Fotonica e Nanotecnologie del Consiglio Nazionale delle Ricerche, Sezione 'FBK-CeFSA' di Trento, Via alla Cascata 56/C, I-38123 Povo (Trento), Italy
[3] Dipartimento di Fisica, Università di Trento, Via Sommarive 14, I-38123 Povo (Trento), Italy

E-mail: sipr@fzu.cz

Received 19 February 2009, in final form 6 May 2009
Published 1 June 2009
Online at stacks.iop.org/JPhysCM/21/255401

Abstract
Cu K-edge x-ray absorption near-edge structure (XANES) spectra of trigonal (3R) $CuScO_2$ and $CuLaO_2$ and of hexagonal (2H) $CuScO_2$ were investigated experimentally and theoretically, in order to study differences between spectra of isostructural and isoelectronic compounds. Significant differences were found in the Cu K-edge XANES of 3R $CuScO_2$ and 3R $CuLaO_2$; these differences can be understood by considering the calculated polarization dependence of the XANES spectra and the differences between the phaseshifts of Sc and La. Spectra of the 3R and 2H polytypes of $CuScO_2$ differ only weakly and the difference originates from the long-range order. The pre-edge peak around 8980 eV is generated by the same mechanism as the pre-edge peak in Cu_2O, i.e. involving scattering by the Cu atoms in the plane which is perpendicular to the O–Cu–O axis.

(Some figures in this article are in colour only in the electronic version)

1. Introduction

X-ray absorption near-edge structure (XANES) is generated via the scattering of a photoelectron by neighbouring atoms. XANES can also provide valuable information about local aspects of low-lying unoccupied electronic states in these systems. In this way, XANES includes information about both atomic and electronic structure. Materials with similar structure and with similar chemical properties are expected to yield similar XANES. This was indeed observed in numerous studies, e.g. spectra of TiS_2, $TiSe_2$ and $TiTe_2$ [1], FeS, CoS and NiS [2] or of ternary chalcogenide semiconductors [3–5].

Recently, delafossites have attracted a lot of attention because they represent a rare example of a p-type transparent conductor, with potential applications in optoelectronics [6, 7]. Another interesting property of delafossites is their negative thermal expansion [8], which has been investigated recently by extended x-ray absorption fine structure (EXAFS) measurements [9]. Delafossites have an AMO_2 composition, with A being usually monovalent Cu or Ag and M being usually either a trivalent transition metal cation or Al and its isoelectronic analogues Ga and In. Delafossites occur in two polytypes, having either a hexagonal crystal system (the polytype is commonly denoted as 2H) or a trigonal crystal system (the polytype is commonly denoted as 3R).

In this work, we analyse Cu K-edge XANES of delafossites $CuScO_2$ and $CuLaO_2$. Trigonal $CuScO_2$ and $CuLaO_2$ are isostructural and isoelectronic (Sc and La belong to the same group of the periodic table), hence their Cu K-edge XANES should be very similar. No significant differences would be expected here. Also trigonal and hexagonal structures of delafossites are very similar when viewed locally from a Cu site. This means that comparing XANES of trigonal and of hexagonal $CuScO_2$ should reveal the effects of small changes of the structure on electronic states as seen from the Cu site.

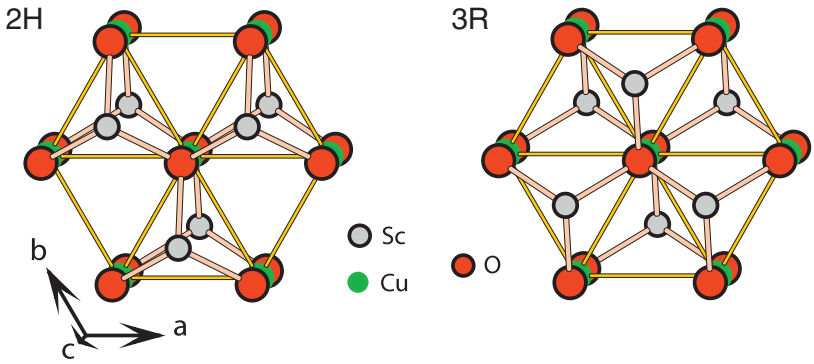

Figure 1. Structural diagrams of the neighbourhood of a Cu atom in the 2H and 3R polytypes of $CuScO_2$ (clusters of 27 atoms are shown). The view is tilted from the *c* axis direction by 7°, meaning that the Cu atoms are nearly completely shielded by the O atoms.

Apart from observing the effects of small variations in the chemistry and in the structure on the XANES, studying delafossites may be helpful in understanding the spectra of other monovalent Cu(I) oxides. Delafossites offer the possibility to study spectra of linearly coordinated monovalent copper with all the O–Cu–O units pointing in the *same direction*. This distinguishes delafossites from, for example, cubic Cu_2O where the O–Cu–O units point in four different directions. (Note that for divalent Cu(II) oxides, the situation is different because of a possible interplay of $3d^9$ and $3d^{10}\underline{L}$ electronic configurations [10, 11]).

The local density of unoccupied states for $E \lesssim 10$ eV was published for $AgInO_2$ and $CuAlO_2$ [12] and for $CuGaO_2$ and $CuInO_2$ [13]. XANES at the $L_{2,3}$-edge of the transition metal M was measured for $AgFeO_2$, $AgCoO_2$ and $AgNiO_2$ [14]. A comprehensive spectroscopic study of $CuAlO_2$ undertaken by Aston *et al* concentrated mostly on occupied states, nevertheless, it included O K-edge and Cu $L_{2,3}$-edge XANES as well [15].

No study of the Cu or Ag K-edge XANES of a delafossite has been published so far. Such a study would probe unoccupied states with a p symmetry with respect to the cation A. These states are more delocalized than the d states probed by the $L_{2,3}$-edge XANES and, consequently, are more sensitive to variations in the crystal structure. Cu K-edge XANES of Cu_2O, which resembles delafossites both because of the presence of monovalent Cu(I) and because of similar local structure around Cu, has been analysed in several studies [16–18]. It was found, among other things, that the intensive pre-edge peak in the Cu K-edge XANES of Cu_2O is connected with transitions to states perpendicular to the O–Cu–O axis [16, 17].

In this work, Cu K-edge XANES of $CuScO_2$ (3R), $CuLaO_2$ (3R) and $CuScO_2$ (2H) was studied both experimentally and theoretically. Interesting and unexpected differences were observed both in the experiment and in the theory. The origin of these differences is analysed and discussed by exploiting concepts of the polarization dependence of the spectra and of the scattering properties of atoms in the investigated compounds. Possible implications for the role of the pre-edge peak in other monovalent Cu compounds are discussed.

2. Methods

2.1. Structure of delafossites

Delafossites are layered materials, containing planar layers of the A cations and layers of distorted edge-sharing MO_6 octahedra. Depending on the orientation of each layer in the stacking, two polytypes can be identified. The stacking of layers in the 3R polytype can be characterized as ABCABC, the crystal has a trigonal (rhombohedral) symmetry and the structure belongs to the space group no. 166 (D^5_{3d}, $R\bar{3}m$). The stacking of layers in the 2H polytype can be characterized as ABAB, the crystal has a hexagonal symmetry and the structure belongs to the space group no. 194 (D^4_{6h}, $P6_3/mmc$). Structural diagrams of clusters of 27 atoms around Cu in both the 2H and 3R polytypes of $CuScO_2$ are presented in figure 1. From these diagrams, one can see how the difference between the 3R and 2H polytypes affects the *local* structure around Cu atoms—which is essential for interpretation of x-ray absorption spectra. Structural diagrams comparing the 3R and 2H polytypes with the emphasis on the long-range order can be found, for example, in [7].

Figure 1 shows the structures viewed parallelly to the *c* axis. Figure 2 shows 15-atom and 27-atom clusters around Cu in the 3R polytype viewed perpendicularly to the *c* axis. It is worth noting that the structure of the 15-atom cluster in delafossites is very similar to the structure of the 15-atom cluster in Cu_2O (provided that one substitutes Cu for the Sc/La atoms). Only after a further 12 oxygen atoms—beyond the 15-atom cluster—have been added, does the difference between the nearest neighbourhood of Cu in delafossites and in Cu_2O start to emerge.

For a quantitative comparison, table 1 shows distances between the central Cu and the nearest O, Cu and M atoms (M stands for Sc in $CuScO_2$, for La in $CuLaO_2$ and for Cu in Cu_2O). When comparing the 3R polytypes, one should note that the distances along the *c* axis are practically the same for $CuScO_2$ and $CuLaO_2$ while the distances in the *ab* plane are by 20% larger for $CuLaO_2$ than for $CuScO_2$, consistently with the larger atomic radius of La.

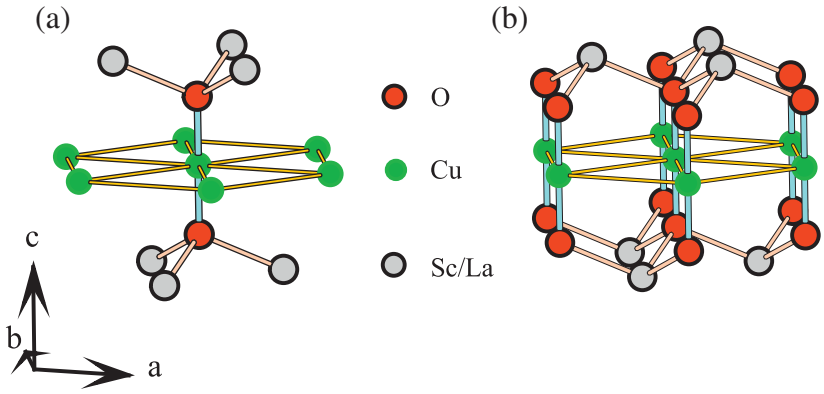

Figure 2. Structural diagrams of the neighbourhood of a Cu atom in 3R $CuScO_2$ or 3R $CuLaO_2$: (a) cluster of 15 atoms, (b) cluster of 27 atoms. The view is tilted from the *ab* plane by 10°.

Table 1. Distances between Cu and its nearest neighbours in $CuScO_2$, $CuLaO_2$ and Cu_2O (see figure 2(a)). The M atom is Sc in $CuScO_2$, La in $CuLaO_2$ and Cu in Cu_2O. The unit is Å. The number of atoms in respective coordination shells around Cu is in the second column (note that for Cu_2O, the Cu–Cu and Cu–M shells in fact form a single shell with 12 atoms).

	N	$CuScO_2$ (2H)	$CuScO_2$ (3R)	$CuLaO_2$ (3R)	Cu_2O
Cu–O	2	1.83	1.80	1.85	1.85
Cu–Cu	6	3.22	3.22	3.83	3.02
Cu–M	6	3.41	3.40	3.61	3.02

2.2. XANES measurements

The synthesis method for the $CuScO_2$ (2H and 3R) and $CuLaO_2$ (3R) powders was described before [19, 20]. Homogeneous samples for XANES measurements were prepared by precipitating fine powders of $CuScO_2$ and $CuLaO_2$ on polytetrafluoroethylene membranes from suspensions in methyl alcohol. Transmission XANES measurements were done at the BM08 (Gilda) beamline of the European Synchrotron Radiation Facility (ESRF) in Grenoble, France. The x-ray beam was monochromatized by two parallel silicon crystals with flat (311) reflecting faces, detuned to reduce the harmonics influence. For energy-scale calibration purposes, the absorption of a copper reference foil placed past the second ionization chamber was measured contemporarily. The spectra presented here were measured at $T = 300$ K.

Further details on measurements and on data analysis can be found in an earlier paper [9], which was dedicated to temperature dependent EXAFS measurements.

2.3. Computational framework

Cu K-edge spectra of 3R $CuScO_2$ and $CuLaO_2$ and of 2H $CuScO_2$ were calculated *ab initio* in a real space via the multiple-scattering technique [21], using the RSMS code [22, 23]. Muffin-tin potentials were taken from self-consistent calculations of the electronic structure of clusters of 24–27 atoms. These calculations were performed using an amended XASCF code [24, 25] which is based on the SCF-$X\alpha$ formalism [26]. Because we are dealing with solids, the clusters have to be effectively embedded in a crystal. That means that while the Schrödinger equation is solved for a molecular cluster, the potential is generated by assuming that the atoms of the cluster are in fact part of a crystal. More specifically, within each self-consistency iteration, atoms in crystallographic positions are attributed the electron densities which were obtained via a SCF-$X\alpha$ calculation for atoms in the molecular cluster, and then the muffin-tin potential of a crystal is generated in a standard way. If more atoms of the same type are present in the cluster, the electron density around that atom which is most centrally located is taken. Only the potential of the outer sphere, which surrounds the cluster and is responsible for the localization of the electronic states in the cluster, is generated as in a standard SCF-$X\alpha$ molecular calculation.

For each of the atomic types in the crystal, a separate SCF-$X\alpha$ calculation is done, with the respective atom in the centre of the cluster. In order to guarantee that the potential generated in this way is free from spurious molecular effects, one can do another series of calculations where the previously obtained electron densities are kept fixed during the self-consistency cycle for all but the most central 3–5 atoms. It turns out that for clusters larger than ∼15 atoms, the resulting potentials do not significantly differ from those obtained during the first set of calculations. We found that this procedure generates potentials which give rise to x-ray spectra that are similar to spectra obtained for potentials found via self-consistent band-structure calculations (see [27] for an example).

The procedure outlined above is not very straightforward. On the other hand, it is quite robust, its speed does not crucially depend on the symmetry of the material and it can handle different systems independently of their electronic properties (metals, semiconductors, ionic compounds). However, its main advantage is that, within the final state approximation, it enables us to account for the core hole. We included it here via the relaxed and screened model (i.e. the electronic structure of the cluster was calculated with one 1s electron removed from the photoabsorbing Cu atom and transferred into the valence states).

The exchange and correlation effects were accounted for via the energy-independent $X\alpha$ potential with the Kohn–Sham value of $\alpha = 0.67$. The muffin-tin radii were set so that

Table 2. Radii of muffin-tin spheres around Cu, Sc, La and O atoms in 2H $CuScO_2$, 3R $CuScO_2$, 3R $CuLaO_2$ and in a hypothetical $CuLaO_2$ with structure of 3R $CuScO_2$. The unit is Å.

	$CuScO_2$ (2H)	$CuScO_2$ (3R)	$CuLaO_2$	$CuLaO_2$ (as $CuScO_2$)
Cu	0.96	0.96	0.96	0.87
Sc/La	1.24	1.24	1.44	1.30
O	0.96	0.92	0.96	0.92

the 'matching potential condition' is satisfied, allowing for an overlap of at most 10% (the values are shown in table 2). The muffin-tin zero was identified with the proper average of the interstitial potential V_{int}, in accordance with our previous experience with XANES of oxides (see, e.g. [28]).

Apart from calculating isotropic polarization-averaged spectra (corresponding to our non-oriented powder samples), we calculated also linearly polarized spectra which correspond to monocrystals. The angular dependence of polarized spectra is determined by the crystal point group. For delafossites, this angular dependence can be described by two independent spectral components. One of these components corresponds to the situation where the x-ray polarization vector $\boldsymbol{\varepsilon}$ is parallel to the c axis, the other one to the situation where $\boldsymbol{\varepsilon}$ is in the ab plane [29].

Theoretical spectra were convoluted by a Lorentzian curve in order to simulate the effect of finite lifetimes of the core hole and of the excited photoelectron. The broadening associated with the core hole lifetime was set to 1.55 eV, according to the compilation of Al Shamma *et al* [30]. The broadening associated with the photoelectron lifetime was set by amending the 'universal curve' of Müller *et al* [31] according to the suggestions of Benfatto *et al* [32] (we assumed a damping associated with one valence electron, starting at the onset energy $E_{\mathrm{s}} = 16$ eV).

Our calculations cannot yield absolute energies of the absorption edges with an accuracy better than ∼1%. Achieving a higher accuracy would require a better treatment of the core hole in a solid while taking into account the p symmetry of the final states. Also, the core electrons would have to be treated fully relativistically. Therefore, we align the energy scale of the theoretical spectra to the experiment by hand so that a good overall agreement between the peak positions in the theory and in the experiment is obtained. Some ambiguity is introduced in this way but it does not matter to the main purpose of this work. As concerns the intensities of the absorption spectra, we scaled the theoretical results so that they match in intensity the experiment at the high-energy tail (above 9040 eV).

2.4. Energy ranges

When comparing XANES of materials which have similar structures but different lattice parameters, one can make use of the fact that interatomic distances enter the XANES formula explicitly only in a product with the photoelectron wavevector $k = \sqrt{E - V_{\mathrm{int}}}$ [23]. That means that if XANES spectra are scaled appropriately, differences due to different lattice constants will be suppressed. More specifically, if two particular spectral features occur at energies E_1 and E_1' for one compound and at energies E_2 and E_2' for another compound, then *neglecting the differences in the phase shifts* one gets

$$(E_1 - E_1')d_1^2 = (E_2 - E_2')d_2^2,$$

where d_1 and d_2 are characteristic interatomic distances in the first and in the second compound, respectively [1]. It is worth noting that this reasoning has a similar basis to the so-called 'Natoli's rule' [33] which has been used in estimating bond lengths in molecular complexes.

If one thus plots the spectrum of each material in its own energy range set according to the kd = const prescription, where d is a typical interatomic distance, the deviations still remaining in the plots are signatures of the differences in the phase shifts $\delta_\ell(E)$. For the purpose of this scaling, we took the characteristic distances $d = 2.336$ Å for 3R $CuScO_2$, $d = 2.341$ Å for 2H $CuScO_2$ and $d = 2.626$ Å for 3R $CuLaO_2$ (based on the unit cell volumes). When studying our plots in the following section, one has to be aware, nevertheless, that even though the use of the kd = const prescription compensates for the differences in the distances d, it does not account for the differences in the c/a ratios (for $CuLaO_2$, the ratio c/a is by 20% smaller than for $CuScO_2$).

3. Results

3.1. Isotropic spectra

The experimental as well as theoretical spectra of powdered 2H $CuScO_2$, 3R $CuScO_2$ and 3R $CuLaO_2$ are shown in figure 3. The theoretical spectra were obtained for clusters of 203 atoms.

One can see that experimental spectra of the two $CuScO_2$ polytypes (2H and 3R) differ only weakly from one another. On the other hand, significant differences occur between the spectra of 3R $CuScO_2$ and 3R $CuLaO_2$. The similarity between the two spectra of $CuScO_2$ and the dissimilarity between the two spectra of the 3R compounds is well accounted for by the theory as well.

The theoretical curves reproduce all significant features of the experiment, albeit sometimes in shifted energy positions and with different peak intensities. As mentioned in section 2.3, the potentials we used for the calculations are self-consistent and include the 1s core hole. We found, nevertheless, that neither the self-consistency nor the core hole are crucial for obtaining a good agreement with the experiment: the difference between the spectra of 3R $CuScO_2$ and 3R $CuLaO_2$ can be reproduced also for non-self-consistent potentials (created according to the so-called Mattheiss prescription) and/or for potentials which neglect the core hole. Interestingly, the distance between the pre-edge peak at 8980 eV and the other peaks is better reproduced in theory for $CuLaO_2$ than for $CuScO_2$—even though there is no obvious reason why the theory should work better for one material than for the other. The agreement between the theoretical and experimental peak positions would probably improve if an energy-dependent exchange–correlation potential was used. However, it is still quite difficult to decide *a priori* which form of the exchange–correlation potential would be most suitable for a particular situation [34–36]. Therefore, we stick with

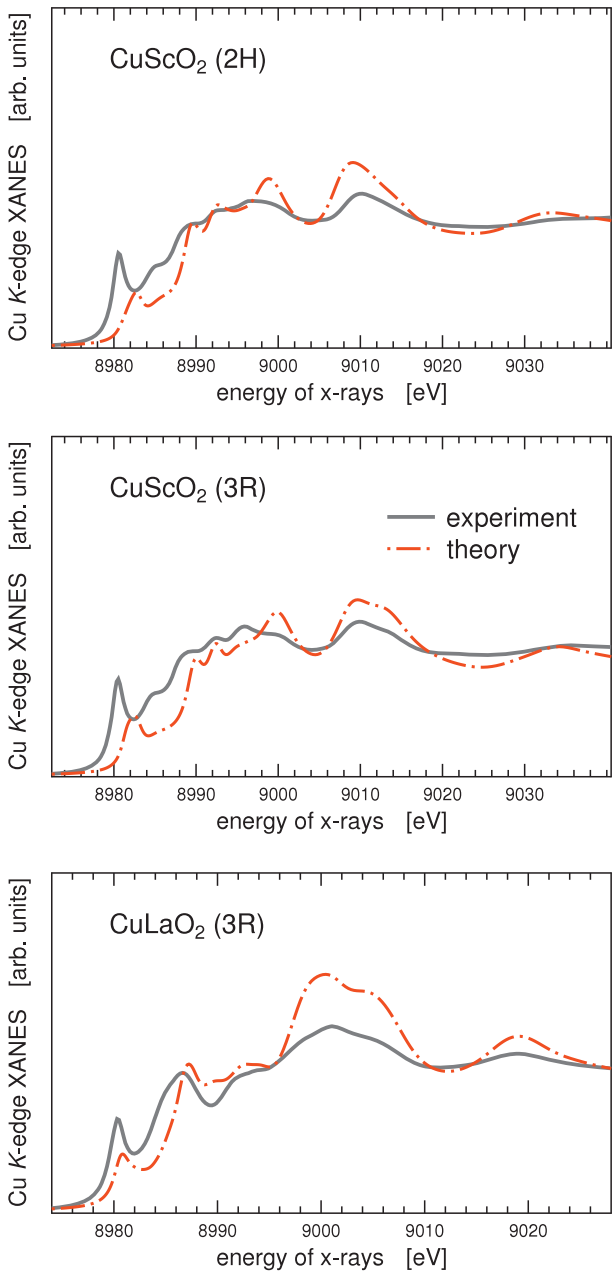

Figure 3. Experimental and theoretical Cu K-edge XANES of 2H and 3R $CuScO_2$ and 3R $CuLaO_2$. Experimental spectra are shown via full lines, theoretical spectra are shown via dash–dotted lines.

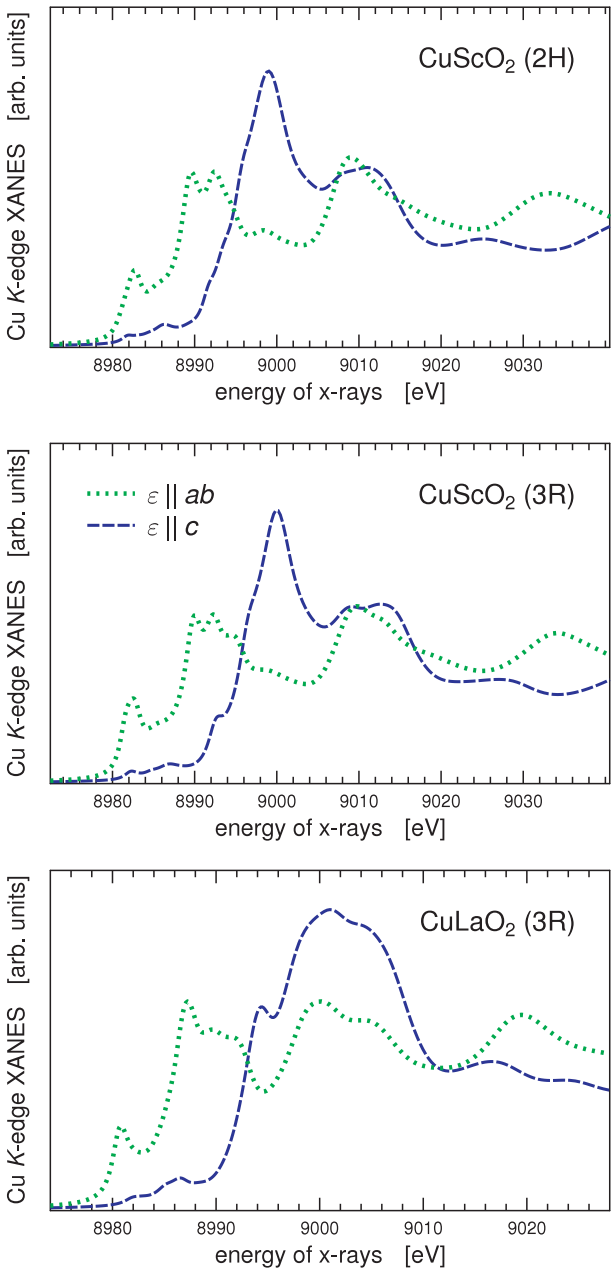

Figure 4. Theoretical polarized Cu K-edge XANES of 2H and 3R $CuScO_2$ and 3R $CuLaO_2$. Spectra for the polarization vector $\boldsymbol{\varepsilon}$ in the *ab* plane are shown via dotted lines, spectra for the polarization vector $\boldsymbol{\varepsilon}$ parallel to the *c* axis are shown via dashed lines. The vertical scales are the same as for analogous plots in figure 3.

the energy-independent $X\alpha$ potential which is sufficient for the purposes of this study.

3.2. Effects of sample orientation

Apart from the isotropic spectra shown in figure 3 (i.e. spectra averaged over all orientations of the polarization vector $\boldsymbol{\varepsilon}$), we calculated also polarized spectra (i.e. considering absorption of linearly polarized x-rays in monocrystals). These spectra are shown in figure 4. Note that the vertical scale of figure 4 is the same as of figure 3 and that the calculations were again performed for clusters of 203 atoms. One can see that the theory predicts quite a large polarization effect. It follows from figure 4 that the $\boldsymbol{\varepsilon} \parallel ab$ components of all the spectra are quite similar while the $\boldsymbol{\varepsilon} \parallel c$ component of the spectrum of 3R $CuLaO_2$ differs from the spectra of $CuScO_2$. The difference between the isotropic Cu K-edge XANES of 3R $CuScO_2$ and 3R $CuLaO_2$ observed in figure 3 comes, therefore, from the $\boldsymbol{\varepsilon} \parallel c$ spectral component.

3.3. Scattering phaseshifts of analogous atoms

The fact that spectra of $CuScO_2$ and $CuLaO_2$ differ may come as surprising, given the fact that Sc and La have similar

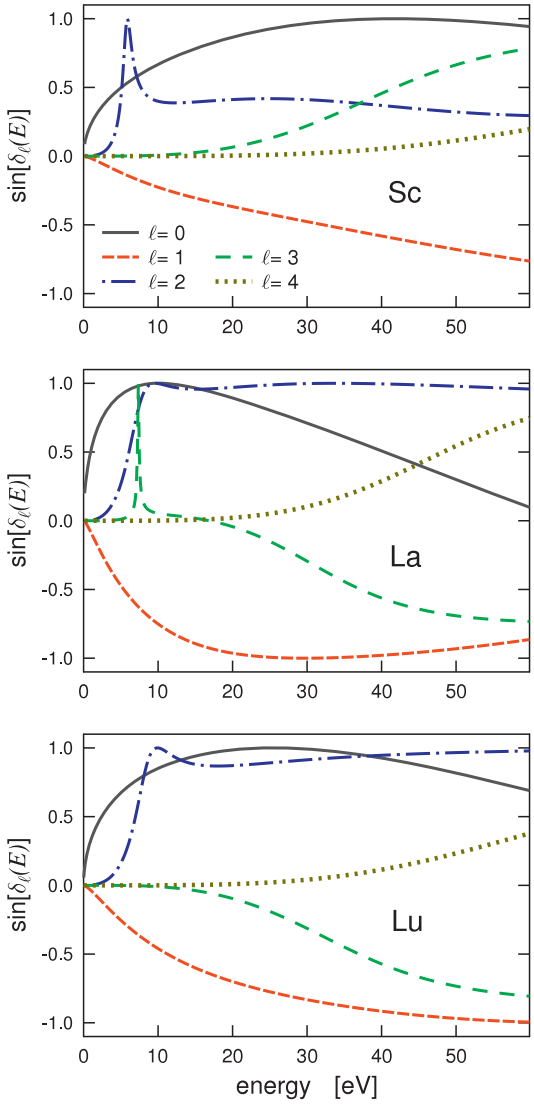

Figure 5. Scattering phase shifts sin[$\delta_\ell(E)$] for Sc in 3R $CuScO_2$ (upper panel), for La in 3R $CuLaO_2$ (middle panel) and for Lu in a hypothetical 3R $CuLuO_2$ (lower panel) for angular momenta $\ell = 0$–4. The horizontal axes represent the photoelectron energy above the muffin-tin zero $V_{\rm int}$; note that, according to the alignment of figure 3, the onset of the conduction band is about 8 eV above $V_{\rm int}$ for $CuScO_2$ and 5.5 eV above $V_{\rm int}$ for $CuLaO_2$.

configuration of valence electrons (Sc $3d^14s^2$, La $5d^16s^2$). A closer look on the scattering properties of Sc and La can be obtained by inspecting the partial-wave phase shifts $\delta_\ell(E)$ (electronic structure enters into XANES calculations via $\delta_\ell(E)$ [21]). Figure 5 shows sin[$\delta_\ell(E)$] for Sc in 3R $CuScO_2$ and for La in $CuLaO_2$. Clearly, phase shifts of Sc and La differ significantly, implying that XANES of $CuScO_2$ and $CuLaO_2$ should differ as well (as observed in figure 3). The difference between Sc and La can be observed also in a more integral quantity, namely, in the scattering cross-section σ (which can be evaluated from the phaseshifts $\delta_\ell(E)$). It turns out that σ for La is about two to three times larger than σ for Sc.

Sometimes it is argued that La should not be considered as an equivalent of Sc among the 5d elements because the empty 4f shell of La may be prone to perturbations. In this line of reasoning, the proper equivalent of Sc should be Lu which has got its 4f shell filled (its electron configuration is $4f^{14}5d^16s^2$). Therefore, we calculated the phaseshifts $\delta_\ell(E)$ also for Lu in a hypothetical $CuLuO_2$ compound obtained just by swapping Lu for La in $CuLaO_2$ while keeping the geometry intact (see the bottom panel of figure 5). One can see that the phase shifts for La and for Lu are quite similar. The only significant difference concerns the sharp resonance for the $\ell = 3$ phaseshifts near the origin: it occurs for La, which is just about to bind a 4f state but not for Lu, where no such binding is expected. This resonance can influence the detailed shape of the pre-peak but otherwise one can expect that XANES spectra of $CuLaO_2$ and of the hypothetical $CuLuO_2$ will be quite similar. We checked this explicitly by performing the corresponding XANES calculations (the results are not shown here for brevity). As a whole, it follows from this test that the difference between scattering properties of Sc and La is *not* simply a consequence of the presence of low-lying empty 4f states in La.

3.4. Role of specific groups of atoms

For a further understanding of the difference between XANES of $CuScO_2$ and $CuLaO_2$ and of the role played by different scatterers, it may be useful to observe how the theoretical spectra change if different groups of atoms are involved in the calculation. Figure 6 shows polarized spectra of 3R $CuScO_2$ and 3R $CuLaO_2$ calculated for clusters of 15, 27 and 203 atoms. The structure of the 15-atom cluster is shown in figure 2(a) and the structure of the 27-atom cluster is shown in figure 2(b). One can see from figure 6 that the most important features of the $\boldsymbol{\varepsilon} \parallel ab$ spectrum can be reproduced for cluster of 27 atoms. In fact, we found that it would be sufficient to use just seven Cu and fourteen O atoms; adding the remaining six Sc/La atoms does not alter the $\boldsymbol{\varepsilon} \parallel ab$ spectrum significantly, indicating thus that for the $\boldsymbol{\varepsilon} \parallel ab$ spectral component, scattering by the Sc or La atoms does not really participate in the formation of the fine structure. Inclusion of the seven Cu atoms and fourteen O atoms is also necessary for the pre-edge peak at 8980 eV to emerge.

For the $\boldsymbol{\varepsilon} \parallel c$ polarization, theoretical spectra of $CuScO_2$ and $CuLaO_2$ differ from one another even for 15-atom clusters. The gross shape of the $\boldsymbol{\varepsilon} \parallel c$ spectrum is reproduced if 27 atoms are included.

The differences between Cu K-edge XANES of 2H $CuScO_2$ and 3R $CuScO_2$ are small; they appeared in our calculations only if more than 100 atoms were taken into account, suggesting that this is a long-range order issue. However, because this difference is small and because the agreement between theory and experiment is not perfect, we cannot be certain that our calculation really reflects the difference between XANES of 2H and 3R $CuScO_2$ properly. Figure 3 suggests, nevertheless, that the difference between XANES of 2H and 3R $CuScO_2$ should be more visible for the $\boldsymbol{\varepsilon} \parallel ab$ polarization.

3.5. Sc–La substitution and differences in the geometry

As noted in section 2.1, trigonal 3R $CuScO_2$ and 3R $CuLaO_2$ differ one from another not only via the Sc–La substitution

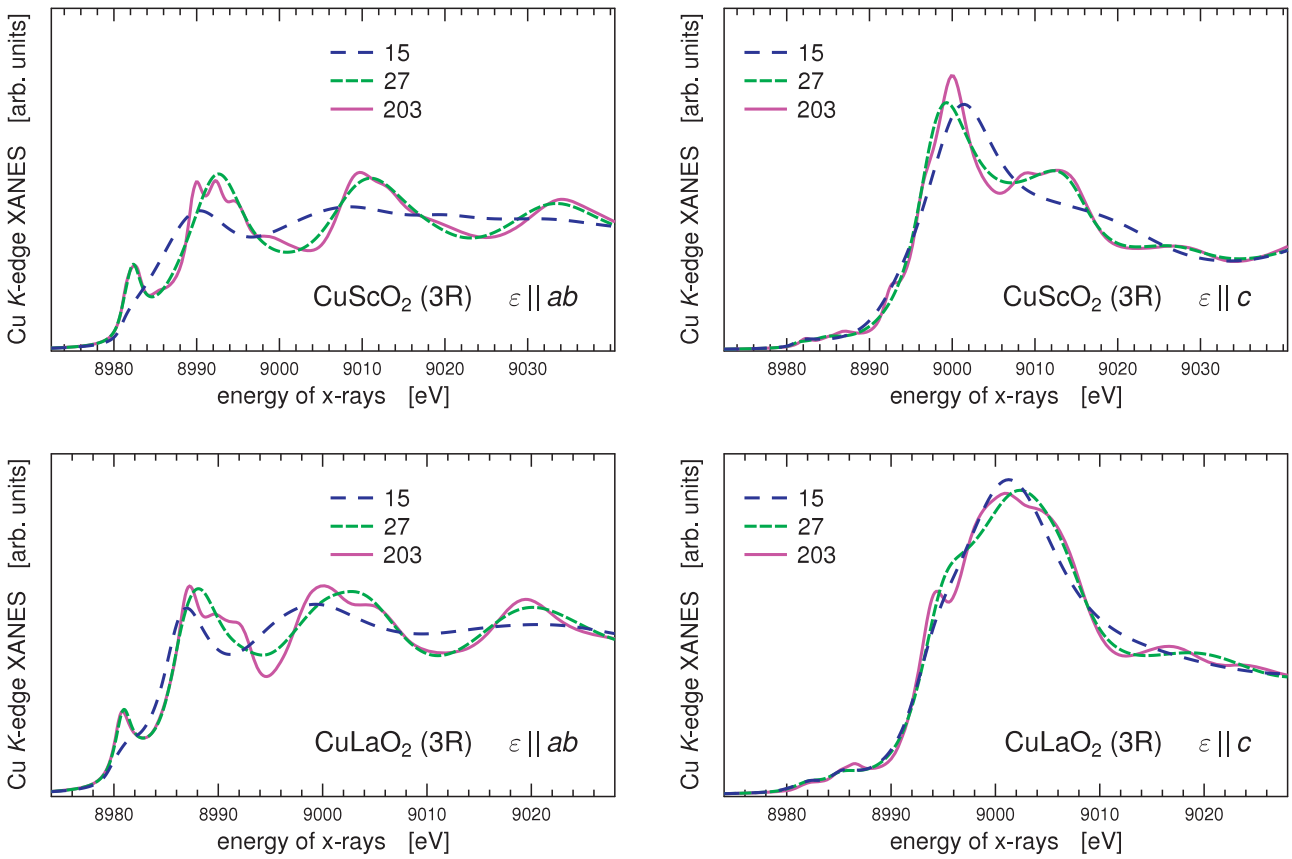

Figure 6. Dependence of polarized Cu K-edge XANES of 3R $CuScO_2$ and 3R $CuLaO_2$ on the atoms included. Polarized spectra calculated for clusters of 15, 27 and 203 atoms are shown for the $\boldsymbol{\varepsilon} \parallel ab$ polarization in the left panels and for the $\boldsymbol{\varepsilon} \parallel c$ polarization in the right panels. Note that the 27-atom and 203-atom curves are sometimes hardly distinguishable from one another.

but also via differences in the geometries (cf the reversed order of Cu–Cu and Cu–M interatomic distances for these two compounds in table 1). In an effort to separate these two effects, we calculated polarized Cu K-edge spectra also for a hypothetical $CuLaO_2$ compound with the geometry taken to be exactly the same as for 3R $CuScO_2$.

The results are shown in figure 7. By comparing figure 7 with figure 4, one can see that the $\boldsymbol{\varepsilon} \parallel ab$ polarization component resembles the $\boldsymbol{\varepsilon} \parallel ab$ spectrum of $CuScO_2$ while the $\boldsymbol{\varepsilon} \parallel c$ component resembles the $\boldsymbol{\varepsilon} \parallel c$ spectrum of the proper $CuLaO_2$. This again stresses the role played by the differences in scattering properties of Sc and La: the $\boldsymbol{\varepsilon} \parallel ab$ component highlights the scattering which involves Cu atoms and O atoms but not Sc or La atoms (cf figure 2 and also the comments regarding figure 6 in section 3.4 above). The scattering amplitudes of Cu and O do not depend very much on whether we are dealing with $CuScO_2$ or with $CuLaO_2$. On the other hand, the distances in the ab plane differ by $\sim$20% between these two compounds (cf table 1). So one can expect that for the $\boldsymbol{\varepsilon} \parallel ab$ component, the geometry will dominate and it is therefore plausible that the $\boldsymbol{\varepsilon} \parallel ab$ spectrum of the hypothetical $CuLaO_2$ with a $CuScO_2$ geometry is similar to the spectrum of $CuScO_2$.

On the other hand, the $\boldsymbol{\varepsilon} \parallel c$ spectral component involves a significant contribution from scattering by Sc or La and it is therefore not surprising that in this case, the effect of a chemical substitution dominates over the geometry.

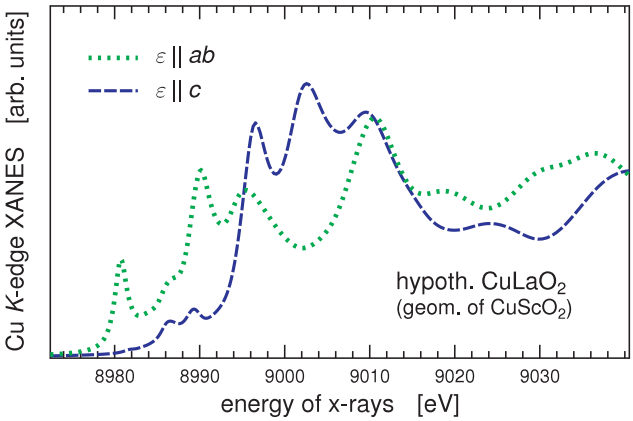

Figure 7. Theoretical polarized Cu K-edge XANES of a hypothetical $CuLaO_2$ with the geometry of 3R $CuScO_2$. This plot is analogous to plots in figure 4.

4. Discussion

By knowing that structurally and chemically similar compounds usually have similar XANES, we have measured and analysed Cu K-edge XANES spectra of trigonal (3R) and hexagonal (2H) polytypes of $CuScO_2$ and of 3R $CuLaO_2$. We have identified quite large differences between the isotropic spectra of isostructural and isoelectronic 3R compounds

$CuScO_2$ and $CuLaO_2$. The calculations show that these differences originate from the differences in the $\boldsymbol{\varepsilon} \parallel c$ polarized spectral component and are consistent with differences in the phase shifts of Sc and La. Spectra of 3R and 2H polytypes of $CuScO_2$ differ only weakly and the difference originates from the long-range order.

Our analysis suggests that different scattering properties of Sc and La are not necessarily connected with the presence of low-lying empty 4f states of the latter. Consequently, it is possible that similar differences in XANES might occur also for isostructural and isoelectronic compounds containing other pairs of 3d–5d metals, such as Ti–Hf or V–Ta.

The differences between XANES of 3R $CuScO_2$ and 3R $CuLaO_2$ appeared much more clearly when polarized spectra were looked on. Polarized spectra thus bear significantly more information than isotropic spectra. Similar conclusions were reached earlier for other copper oxides such as CuO [37] or $CuGeO_3$ [38].

Our finding that the difference between spectra of 3R $CuScO_2$ and $CuLaO_2$ is much more pronounced for the $\boldsymbol{\varepsilon} \parallel c$ polarization than for the $\boldsymbol{\varepsilon} \parallel ab$ polarization is consistent with the changes in the local environment of Cu in these compounds: Sc and La atoms, for which the phase shifts differ significantly, are located quite far from the ab plane defined by Cu hexagons and thus will be more involved in the $\boldsymbol{\varepsilon} \parallel c$ polarized spectra than in the $\boldsymbol{\varepsilon} \parallel ab$ polarized spectra.

The distinct pre-edge peak at 8980 eV appears in the calculations for the $\boldsymbol{\varepsilon} \parallel ab$ polarization only. This reminds us of the situation with Cu_2O, where it was similarly found that the pre-edge peak is connected with transitions perpendicular to the O–Cu–O axis [16, 17]. However, unlike in the case of Cu_2O, the O–Cu–O chains are all parallel to each other in a delafossite crystal, meaning that the association between the pre-edge peak and states in the ab plane could be, in principle, demonstrated by experiment (if a monocrystal sample is used).

Our analysis of the polarization dependence of Cu K-edge XANES of delafossites shows that the formation of the pre-edge peak involves scattering by Cu atoms in the ab plane (as well as by O atoms which linearly coordinate these Cu atoms in a direction perpendicular to the plane containing Cu atoms). A similar conclusion could be drawn locally also for Cu_2O [17]. The fact that scattering by atoms in the ab plane is involved in the formation of the Cu K-edge pre-peak cannot, however, be generalized. Such a pre-peak, namely, appears also in systems containing linearly coordinated monovalent Cu where there are no Cu atoms present in the ab plane [39] (e.g. in $[Cu(xypz)]_2(BF_4)_2$ [40]). Thus, it appears that there will be two kinds of pre-peak in monovalent copper compounds; one that involves scattering by Cu atoms in the ab plane (the case of Cu_2O and delafossites) and another one that does not involve this scattering (the case of some molecular complexes studied by Kau *et al* [39]). In support of this conjecture, one can recall that earlier experimental studies observed that the pre-edge peak in Cu K-edge XANES of Cu_2O does not in fact follow the systematic pattern set by the molecular complexes [39, 41].

Generally, our study shows that isostructural and isoelectronic compounds can still have different XANES spectra. This difference could be better identified in polarized spectra.

5. Conclusions

We found that apparent chemical and structural similarity of two compounds (in our case, 3R $CuScO_2$ and 3R $CuLaO_2$) does not necessarily imply that their XANES spectra will be very similar.

The difference between Cu K-edge XANES of isostructural and isoelectronic compounds 3R $CuScO_2$ and 3R $CuLaO_2$ can be understood if one focuses on the polarization dependence of the spectra. The calculations indicate that XANES of 3R $CuScO_2$ and 3R $CuLaO_2$ is similar if the polarization vector $\boldsymbol{\varepsilon}$ of the incoming x-rays lies in the ab plane while it significantly differs if $\boldsymbol{\varepsilon}$ is parallel to the c axis. This behaviour is consistent with different scattering properties of Sc and La.

The pre-edge peak which appears in the XANES of delafossites around 8980 eV is connected with scattering of the photoelectron by at least seven Cu atoms in the ab plane and fourteen O atoms which linearly coordinate these seven Cu atoms. The pre-peak is present only in the $\boldsymbol{\varepsilon} \parallel ab$ polarized component. In this respect the situation is analogous to the case of Cu K-edge XANES of Cu_2O.

Differences between experimental Cu K-edge XANES spectra of the 2H and 3R polytypes of $CuScO_2$ are small. Theoretical analysis indicates that this difference is of long-range-order character.

Acknowledgments

This work was supported by the GA AV project IAA100100514. The research in the Institute of Physics AS CR was supported by the project AV0Z-10100521 of AV ČR. We are grateful to J Li and A W Sleight, who produced and kindly sent us the powdered samples, and to S I Ahmed, M Vaccari and A Sanson, who participated to the XANES measurement runs. We acknowledge the European Synchrotron Radiation Facility (ESRF) for provision of synchrotron radiation facilities and financial support (project HS-3074), as well as F Bardelli and the staff of the BM08-Gilda beamline for technical assistance.

References

[1] Bocharov S, Dräger G, Heumann D, Šimůnek A and Šipr O 1998 *Phys. Rev.* B **58** 7668
[2] Soldatov A V, Kravtsova A N, Fleet M E and Harmer S L 2004 *J. Phys.: Condens. Matter* **16** 7545
[3] Sainctavit P, Petiau J, Flank A M, Ringeissen J and Lewonczuk S 1989 *Physica* B **158** 623
[4] Šipr O, Machek P, Šimůnek A, Vackář J and Horák J 1997 *Phys. Rev.* B **56** 13151
[5] Bacewicz R, Wolska A, Lawniczak-Jablonska K and Sainctavit P 2000 *J. Phys.: Condens. Matter* **12** 7371
[6] Ingram B J, Gonzalez G B, Kammler D R, Bertoni M I and Mason T O 2004 *J. Electroceram.* **13** 167
[7] Marquardt M A, Ashmore N A and Cann D P 2006 *Thin Solid Films* **496** 146
[8] Li J, Sleight A W, Jones C Y and Toby B H 2005 *J. Solid State Chem.* **178** 285
[9] Ahmed S I, Dalba G, Fornasini P, Vaccari M, Rocca F, Sanson A, Li J and Sleight A W 2009 *Phys. Rev* B **79** 104302

[10] Wu Z Y, Benfatto M and Natoli C R 1996 *Phys. Rev.* B **54** 13409
[11] Chaboy J, Muñoz-Páez A and Sánchez Marcos E 2006 *J. Synchrotron Radiat.* **13** 471
[12] Lalic M V, Mestnik-Filho J, Carbonari A W and Saxena R N 2004 *Braz. J. Phys.* **34** 611
[13] Makhova L, Wett D, Lorenz M and Konovalov I 2006 *Phys. Status Solidi* a **203** 2861
[14] Lee S S, Kim J H, Wi S C, Kim G, Kang J S, Shin Y J, Han S W, Kim K H, Song H J and Shin H J 2005 *J. Appl. Phys.* **97** 10A309
[15] Aston D J, Payne D J, Green A J H, Egdell R G, Law D S L, Guo J, Glans P A, Learmonth T and Smith K E 2005 *Phys. Rev.* B **72** 195115
[16] Guo J, Ellis D E, Goodman G L, Alp E E, Soderholm L and Shenoy G K 1990 *Phys. Rev.* B **41** 82
[17] Šipr O 1992 *J. Phys.: Condens. Matter* **4** 9389
[18] Vinogradov A S, Akimov V N and Preobrazhenskii A B 1996 *Opt. Spektrosk.* **81** 807
[19] Li J, Yokochi A, Amos T G and Sleight A W 2002 *Chem. Mater.* **14** 2602
[20] Li J, Yokochi A F T and Sleight A W 2004 *Solid State Sci.* **6** 831
[21] Vvedensky D D 1992 *Unoccupied Electron States* ed J C Fuggle and J E Inglesfield (Berlin: Springer) p 139
[22] Šipr O 1996–1999 *Computer Code* RSMS Institute of Physics AS CR, Prague
[23] Vvedensky D D, Saldin D K and Pendry J B 1986 *Comput. Phys. Commun.* **40** 421
[24] Cook M and Case D A 1980 *Computer Code* XASCF Quantum Chemistry Program Exchange, Indiana University, Bloomington
[25] Šipr O, Rocca F and Dalba G 1999 *J. Synchrotron Radiat.* **6** 770
[26] Johnsson K H 1973 *Adv. Quantum Chem.* **7** 143
[27] Šipr O and Šimůnek A 2001 *J. Phys.: Condens. Matter* **13** 8519
[28] Šipr O, Šimůnek A, Bocharov S, Kirchner T and Dräger G 1999 *Phys. Rev.* B **60** 14115
[29] Brouder C 1990 *J. Phys.: Condens. Matter* **2** 701
[30] Shamma F A, Abbate M and Fuggle J C 1992 *Unoccupied Electron States* ed J C Fuggle and J E Inglesfield (Berlin: Springer) p 347
[31] Müller J E, Jepsen O and Wilkins J W 1982 *Solid State Commun.* **42** 365
[32] Benfatto M, Della Longa S and Natoli C R 2003 *J. Synchrotron Radiat.* **10** 51
[33] Natoli C R 1984 *EXAFS and Near Edge Structure III* ed K O Hodgson and J Penner-Hahn (Berlin: Springer) p 38
[34] Chaboy J and Quartieri S 1995 *Phys. Rev.* B **52** 6349
[35] Ankudinov A L 1999 *J. Synchrotron Radiat.* **6** 236
[36] Hatada K and Chaboy J 2007 *Phys. Rev.* B **76** 104411
[37] Bocharov S, Kirchner T, Dräger G, Šipr O and Šimůnek A 2001 *Phys. Rev.* B **63** 045104
[38] Šipr O, Šimůnek A, Bocharov S and Dräger G 2002 *Phys. Rev.* B **66** 155119
[39] Kau L S, Spira-Solomon D J, Penner-Hahn J E, Hodgson K O and Solomon E I 1987 *J. Am. Chem. Soc.* **109** 6433
[40] Sorrell T N and Jameson D L 1983 *J. Am. Chem. Soc.* **104** 2053
[41] Moen A, Nicholson D and Ronning M 1995 *J. Chem. Soc. Faraday Trans.* **91** 3189